JOURNAL OF CATALYSIS 70, 323–334 (1981)

Physical Characterization of Fe/TiO_2 Model Supported Catalysts

II. Electron Spectroscopic Studies of Reduction Behavior

B. J. TATARCHUK[1] AND J. A. DUMESIC[2]

Department of Chemical Engineering, University of Wisconsin, Madison, Wisconsin 53706

Received December 2, 1980; revised April 3, 1981

X-Ray photoelectron spectroscopy (XPS) and conversion electron Mössbauer spectroscopy (CEMS) have been used to characterize Fe/TiO_2 model supported catalysts following hydrogen reductions at progressively higher temperatures. Reduction at temperatures near 707 K converted the initially present Fe^{3+} and Fe^{2+} into metallic iron. After further treatment at 773 K, the metallic iron peaks in the Mössbauer spectrum were observed to broaden, consistent with the spreading of iron crystallites over the support. Upon reduction at temperatures of ca. 875 K or higher, decreases were seen in the XPS and CEMS spectral iron areas. In addition, CEMS indicated the formation of a new, metallic species that did not show magnetic hyperfine splitting at room temperature, and XPS indicated that part of the Ti^{4+} was reduced to lower valence states. These results suggest that hydrogen treatment at these temperatures leads to a reduction of the support and to the diffusion of iron into the support, as a dispersed and strongly interacting species (e.g., γ-Fe: Fe_xTi, $1 \leq x \leq 2$).

INTRODUCTION

Part I of this series dealt with the electron microscopic characterization of Fe/TiO_2 model supported catalysts following hydrogen reduction treatments at progressively higher temperatures. Nucleation and growth of the iron particles were observed at temperatures of 608 and 707 K, respectively. In addition, the occurrence of crystallite spreading over or wetting the support surface was seen at 773 K, as found by other investigators for Pt on titania (*1*, *2*). After reduction at or above 875 K, however, a decrease was observed in the amount of iron present as distinct iron particles per unit area of titania surface. This was attributed to the formation of an iron phase that was not detectable by transmission electron microscopy (TEM), created by the "diffuse" spreading of iron over the support or the diffusion of iron into the support. In the present study, these phenomena will be studied further using electron spectroscopic techniques, namely, X-ray photoelectron spectroscopy (XPS) and conversion electron Mössbauer spectroscopy (CEMS). It will be seen that the combination of morphological information from TEM with the electronic, structural, and magnetic insights of *combined* XPS and CEMS studies provides detailed information about the nature of metal-support interactions for Fe/TiO_2. Indeed, CEMS provides information about the chemical properties of iron on and far below the surface, while XPS can be used to study the concentrations and chemical properties of nearly all the elements on or near the surface.

EXPERIMENTAL

Sample Preparation and Treatment

Samples used for XPS and CEMS studies were fabricated according to the methods described in Part I of this series (*3*). In short, these samples were prepared by the evaporation of iron overlayers (enriched to 91% with ^{57}Fe) onto TiO_2 films that had been thermally grown on Ti foils. Two series of samples were prepared, with iron

[1] Present address: Department of Chemical Engineering, Auburn University, Auburn, Alabama 36849.

[2] To whom correspondence should be addressed; Camille and Henry Dreyfus Foundation Teacher-Scholar.

0021-9517/81/080323-12$02.00/0

overlayer thicknesses of 3.8 and 5 nm, respectively, as discussed in Part I. Following deposition of iron onto the TiO_2 films, XPS revealed that the equivalent of about two monolayers of carbon was on the surface of the samples. This carbon signal, however, decreased markedly after hydrogen treatment at ca. 700 K. No other impurities in the samples could be detected by Auger electron spectroscopy (AES), XPS, or CEMS. To facilitate comparison of results from the different techniques, sample treatments for XPS and CEMS studies were essentially identical to those described in Part I for the TEM studies. Differences in the total pressure used during treatment, between the fixed levels of 1.33×10^{-2} Pa for TEM and XPS, and 1.33×10^{-3} Pa for CEMS, were ascertained to be of little consequence. Specifically, TEM experiments employing different total pressures between 101 kPa and 1.33×10^{-3} Pa revealed no differences in the phenomenological behavior of the iron particles. The hydrogen-to-water ratio may affect reduction equilibria, however, and as such it was strictly monitored and controlled at a value of 100: 1, respectively. Finally, to further preserve the similarity of treatment conditions, TEM and XPS specimens were treated in the same reactor chamber, adjacent to the XPS analysis chamber, as discussed below.

XPS Studies

X-Ray photoelectron spectroscopy was performed in the apparatus depicted schematically in Fig. 1 (Physical Electronics, model 548 ESCA/Auger electron spectrometer). With the UHV gate valve closed and the sample rod drawn into the reaction chamber, specimens mounted on the front of the sample rod were reduced in hydrogen at 1.3×10^{-2} Pa and temperatures up to 973 K. During these treatments, hydrogen was introduced into the chamber through a variable UHV leak valve and pumped from the chamber using a turbomolecular pump (Balzers). Typical background pressures in

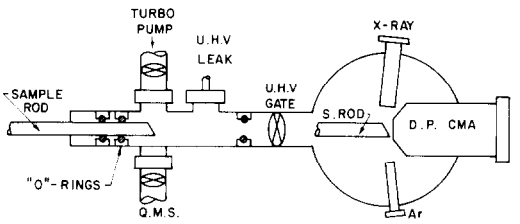

FIG. 1. Schematic diagram of X-ray photoelectron spectrometer with contiguous reaction chamber. Ar, argon sputtering gun; D.P. CMA, double-pass cylindrical mirror analyzer; X-RAY, aluminum X-ray source; U.H.V. GATE, ultrahigh vacuum gate valve; LEAK, leak valve; TURBO PUMP, turbomolecular pump; Q.M.S., quadrupole mass spectrometer.

this reaction chamber were approximately 1.3×10^{-5} Pa, and consisted primarily of H_2O, N_2, O_2, and CO_2 as measured by a quadrupole mass spectrometer (UTI-100C). No hydrocarbons could be detected in the chamber, putting their pressures at less than 10^{-9} Pa. Following treatments, the samples were cooled to room temperature in hydrogen, before stopping the supply of hydrogen to the reaction chamber (by closing the UHV leak valve) and inserting the sample rod into the XPS/AES analysis chamber. Background pressures in the analysis chamber were approximately 1×10^{-7} Pa, and excitation was accomplished using an aluminum source anode.

CEMS Studies

CEMS was performed in the high vacuum chamber depicted in Fig. 2. Shown there is the top view of a chamber that incorporates molecular beam reactive scattering, temperature-programmed desorption (TPD), AES (Physical Electronics 10-155 CMA), and CEMS. For the present discussion, however, it is only the CEMS capabilities that are of importance. The total background pressure in this chamber is approximately 1×10^{-7} Pa as measured against a calibrated quadrupole mass spectrometer (UTI-100C). Pumping is accomplished using a liquid nitrogen-trapped diffusion pump (6 in., T.M. Vacuum Products) with polyphenyl ethers as the pumping fluid

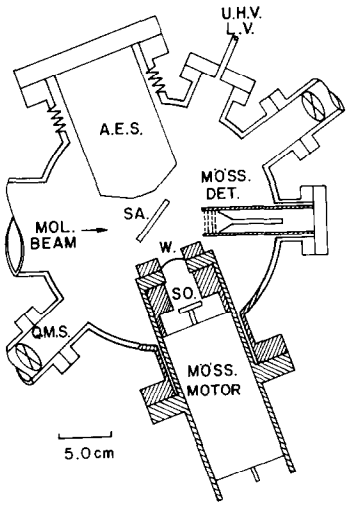

FIG. 2. Schematic diagram of conversion electron Mössbauer spectrometer. MÖSS MOTOR, Doppler velocity transducer; SO., $^{57}Co/Pd$ γ-ray source; W., Teflon-coated Kapton γ-ray window; SA., sample; MÖSS DET., electron detector; U.H.V. L.V., ultrahigh vacuum leak valve; A.E.S., Auger electron spectrometer; MOL. BEAM, molecular beam axis; Q.M.S., quadruple mass spectrometer.

(Santovac-5). Both the diffusion pump and a precision sample manipulator are not shown in Fig. 2 as they lie respectively below and above the plane of the Figure. The sample (ca. 5 × 5 cm), affixed to the manipulator, can be rotated into position for CEMS characterization (as shown in Fig. 2) or positioned for TPD, AES, or molecular beam studies. With this geometry the conversion electron takeoff and γ-ray incidence angles for CEMS can be varied, while the angle between the source and detector axes is fixed.

Samples for study by CEMS were attached to the front of a thick titanium plate (~5 cm × 5 cm × 4 mm) which was heated from the back by tungsten filaments. This thick plate provided isothermicity across the sample as determined by optical pyrometry, while temperature measurement was accomplished using a fine thermocouple just touching the center of the back of the specimen foil. Foil temperatures during sample treatments were controlled to a precision of ±5 K (Valley Forge Instruments). Following the various hydrogen treatments, samples were always cooled to room temperature before closing the UHV leak valve through which hydrogen was introduced into the chamber. CEMS was subsequently carried out with the sample at room temperature.

Mössbauer spectroscopy was conducted using an Austin Science Associates' S-600 spectrometer and K3 electromechanical transducer to provide Doppler velocity modulation of a 25-mCi source of ^{57}Co in palladium. Source photons entered the vacuum system through a 0.127-mm-thick Teflon-coated Kapton window (Dupont), and this radiation was collimated by appropriate brass and stainless-steel shieldings such that photon impingement occurred primarily on the sample surface (see Fig. 2). The internal conversion and subsequent Auger electrons that were then emitted from the sample were detected by a continuous dynode electron multiplier ("Spiraltron"—Galileo Electro-Optics Corporation) and the current pulses from this device (gain $\geq 10^6$) were converted into TTL pulses by a pulse amplifier discriminator (PAD 400-Galileo Electro-Optics Corporation). Pulses (or counts) were then recorded in a synchronous manner with respect to the Doppler velocity of the ^{57}Co source using a multichannel analyzer (MCA—Tracor Northern TN-1705). After collection of approximately 10^5 counts per channel, plotting the number of counts collected in each channel versus the corresponding Doppler velocity for each channel generates the conversion electron Mössbauer spectrum. For the series of samples derived from the 5-nm overlayer of iron on titania, it took approximately 48 h to collect ca. 2 × 10^5 counts in each of the 1024 channels of the MCA with a spectral area of ca. 20% mm/s. To achieve maximum count rate (and to minimize spectral collection time) the ^{57}Co source was positioned as close to the sample as possible. This produced a broadening of measured Möss-

bauer peaks due to the so-called cosine broadening effect (*4*). For this reason, the full widths at half-maximum of the resulting Mössbauer spectral peaks are about five times larger than the minimum theoretical value (i.e., approximately 1 versus 0.19 mm/s).

Following collection of the Mössbauer spectrum, the data (number of counts in each channel) were transferred directly from the MCA to a PDP-11/55 computer. The spectra, collected using a triangular Doppler velocity waveform, were folded and fitted using the program MFIT (*5*). This program fits the data to an assigned number of Lorentzian lines superimposed on a horizontal baseline. The fitting is "least squares" employing a random stepping of free parameters to find the best fit. Doppler velocity was calibrated with a 0.1-mil foil of iron (enriched to 91% in ^{57}Fe), and isomer shifts are reported relative to this standard absorber. Positive velocity corresponds to the source moving toward the absorber.

RESULTS/DISCUSSION

XPS Studies

All XPS studies were performed on pairs of samples. Specifically, a TiO_2 film and a sample consisting of an iron overlayer on a TiO_2 film were mounted at adjacent positions on the tip of the sample rod. In this way, the behaviors of Fe/TiO_2 and of TiO_2 itself could be monitored. Charging effects during XPS studies were not observed to either shift or broaden any spectral features during analysis, probably due to the presence of the metallic Ti foil beneath the TiO_2 films. The binding energy regions studied in detail and reported here were the 10-eV interval around the Fe-$2p_{3/2}$ peak and the 20-eV interval around the Ti-$2p_{3/2}/2p_{1/2}$ doublet. Additionally, 0 to 1000-eV survey scans and 10-eV scans around both C-1*s* and O-1*s* were measured in order to quantitatively determine surface stoichiometries. Calibration of these binding energy scales was performed using the peak shift of the O-1*s* line (530.0) as well as the known positions of the Fe-$2p_{3/2}$ peak for Fe^0, Fe^{2+}, and Fe^{3+} (706.8, 709.5, and 710.7 eV, respectively) and the positions of the Ti-$2p_{3/2}/2p_{1/2}$ doublets for Ti^{4+} (458.5 and 464.2 eV) and Ti^0 (453.8 and 460.0 eV). Further, all spectrometer settings and the sample–analyzer position were held constant to permit direct comparison of spectra following various reduction treatments.

Fe-$2p_{3/2}$ region. The XPS scans of the Fe-$2p_{3/2}$ region after progressively higher reduction treatments are shown in Figs. 3 and 4 for the 5.0- and 3.8-nm iron samples, respectively. Consider first the 5.0-nm iron sample. It can be seen in Fig. 3 that essentially all of the iron (observable by XPS) is reduced to the metallic state during the first two hydrogen treatments at 608 and 643 K. For clarity, the expected peak positions for Fe^0, Fe^{2+}, and Fe^{3+} are indicated on the abscissa of this figure. In addition, it can be seen that the $2p_{3/2}$ spectral area decreases markedly following reduction at temperatures near or above 773 K. Indeed, the results of TEM discussed in Part I of this series rule out the sintering of iron as a possible cause for this decrease in spectral area. Instead, analysis of the electron micrographs after hydrogen treatment at temperatures above 773 K suggested a "diffuse" spreading of iron over the surface or a diffusion of iron into the support. The results of XPS now suggest that it is the latter phenomenon that takes place during high-temperature treatment of the 5-nm iron sample.

Figure 4, for the 3.8-nm iron overlayer, shows similar decreases in the spectral area of the Fe-$2p_{3/2}$ peak after reduction at temperatures in excess of 773 K. Thus, the 5-nm and 3.8-nm series of samples show the same behavior with respect to the diffusion of iron into the titania. By comparison with the 5-nm sample, however, the 3.8-nm iron overlayer on TiO_2 appears to be more difficult to reduce to the metallic state. This is shown by the greater relative amounts of Fe^{2+} in the spectra of Fig. 4, compared to

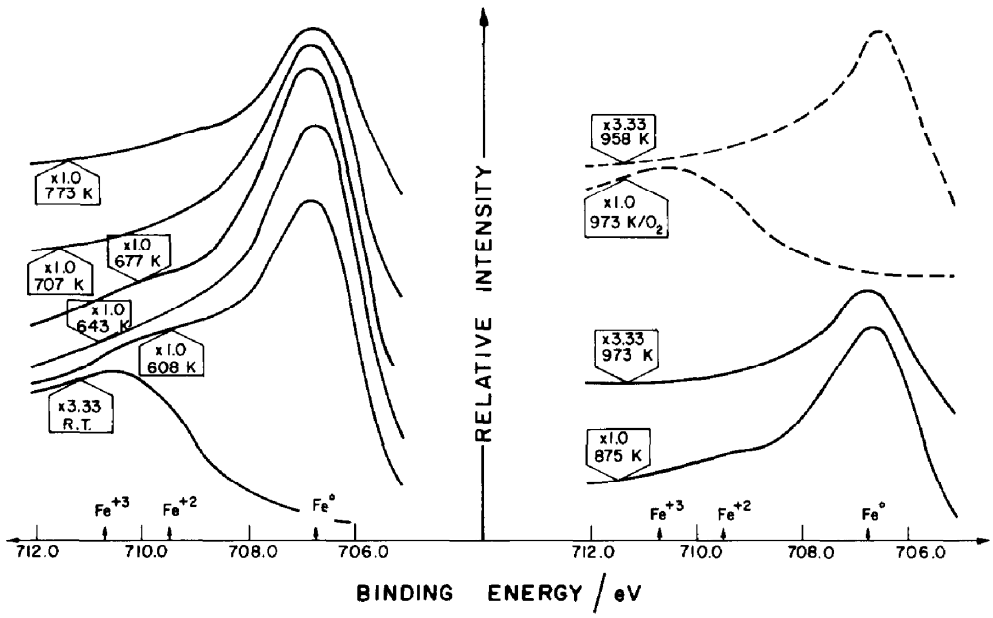

FIG. 3. Fe-$2p_{3/2}$ X-ray photoelectron spectra recorded from 5-nm Fe/TiO_2 specimen after reduction at the indicated temperatures. Vertical sensitivities for each spectrum are shown adjacent to the reduction temperature. Broken spectra were obtained after subsequent oxidation, and they are discussed in Part III of this series. (RT, initial iron overlayer)

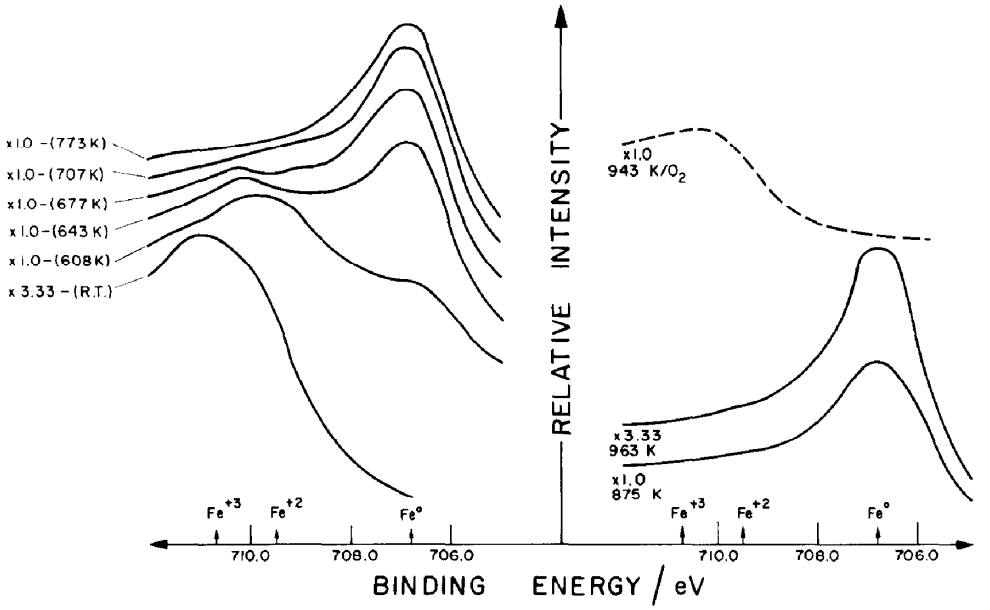

FIG. 4. Fe-$2p_{3/2}$ X-ray photoelectron spectra recorded from 3.8-nm Fe/TiO_2 specimen after reduction at the indicated temperatures. Vertical sensitivities for each spectrum are shown adjacent to the reduction temperature. Broken spectra were obtained after subsequent oxidation, and they are discussed in Part III of this series. (RT, initial iron overlayer)

Fig. 3. Since both 3.8 and 5.0 nm represent high iron loadings, these differences in behavior are believed to arise from the sampling depth of the XPS experiment (ca. 2 nm). For the 5-nm iron overlayer, XPS monitors primarily that portion of the overlayer that is not in contact with TiO_2; while for the 3.8-nm iron overlayer, a greater contribution to the photoelectron spectrum comes from iron that is near the TiO_2 interface. Furthermore, even after nucleation of the iron film into discrete particles (at temperatures above about 677 K), the iron particle size from the 3.8-nm overlayer is on the average smaller than that from the 5.0-nm overlayer (see Part I). In this case as well, the photoelectron spectrum for the 3.8-nm sample should be more sensitive to iron atoms near TiO_2 than is the photoelectron spectrum for the 5-nm sample. Thus, the greater difficulty in reducing the iron to the metallic state in the 3.8-nm sample (as judged by XPS) reflects a stabilization of Fe^{2+} in contact with TiO_2. Indeed, similar conclusions have been reached for iron supported on SiO_2, Al_2O_3, and MgO (*6*).

Ti-2$p_{3/2}$/2$p_{1/2}$ region. Additional information about the interaction between iron and titania is found in the Ti-2$p_{3/2}$/2$p_{1/2}$ region of the photoelectron spectra collected after progressively higher reduction treatments. These are shown in Fig. 5 for a blank titania film and for a titania film initially covered by the 5-nm iron overlayer. For both samples, the titanium appears to be present primarily as Ti^{4+} after reduction at 773 K, the temperature at which the iron was observed to spread over or wet the titania surface (Part I). Reduction at 875 K, however, produces a new component in the

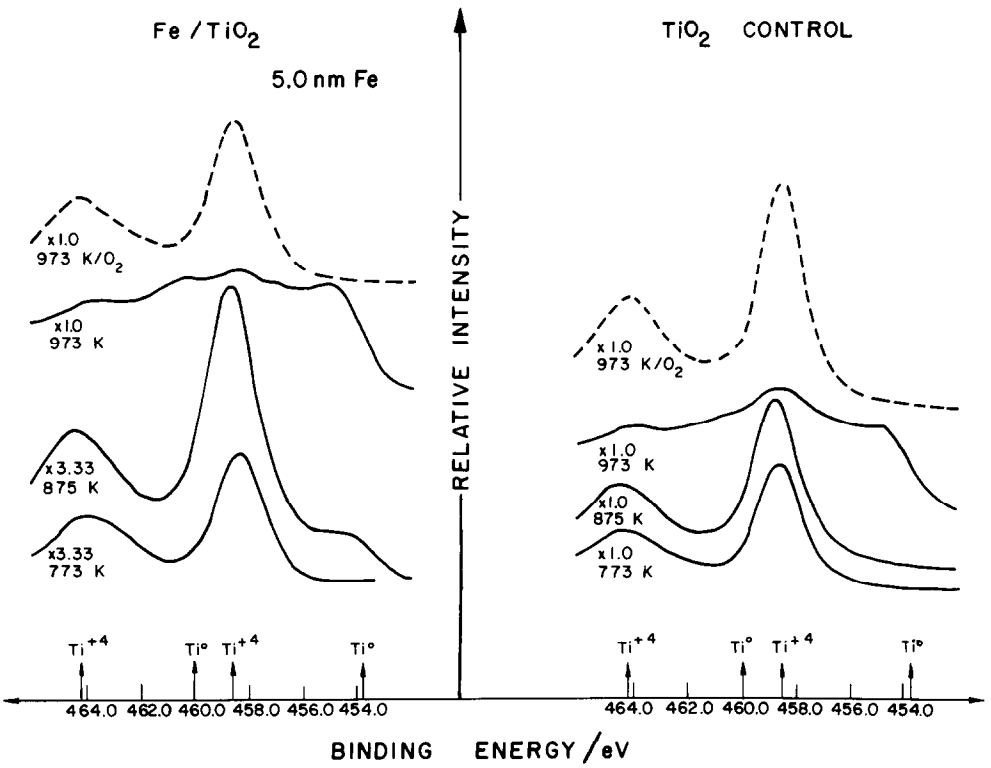

FIG. 5. Ti-2$p_{3/2}$/2$p_{1/2}$ X-ray photoelectron spectra recorded from 5-nm Fe/TiO_2 and Fe-free TiO_2 specimens after reduction at the indicated temperatures. Vertical sensitivities for each spectrum are shown adjacent to the reduction temperature. Broken spectra were obtained after subsequent oxidation, and they are discussed in Part III of this series.

photoelectron spectrum of the iron-containing sample, identifiable by the Ti-$2p_{3/2}$ peak close to the positions of Ti^0 (453.8 eV) and Ti^{2+} (454.8 ± 0.2 eV) (*7–9*). This new component is not present in the spectrum of the titania film itself after treatment in hydrogen at 875 K. The lower binding energy of this new titanium component, compared to Ti^{4+}, indicates that a portion of the TiO_2 in the iron-containing sample has been reduced during treatment in hydrogen at 875 K. Thus, it appears that the presence of iron facilitates the reduction of titania. In separate experiments, photoelectron spectra identical in appearance to the iron-containing specimen at 875 K could be obtained by exposing high-purity Ti metal foils to air at room temperature. In this case, as in Fig. 5, reduced titanium species were observed, corresponding to the weak peak at ca. 455 eV. This peak can be attributed to the presence of titanium in intermediate oxidation states (e.g., Ti^{3+}, Ti^{2+}), and to an apparent shift of the metallic Ti peak due to its presence on the tail of the more intense Ti^{4+} peak (*10, 11*).

The photoelectron spectra of Fig. 5 also indicate that the surface of the TiO_2 film itself (in the absence of iron) can be partially reduced when the temperature is raised further to 973 K. This reduction might be related to the restructuring of the TiO_2 film that was observed in Part I to take place at temperatures near 973 K. Alternatively, it may be dependent on the presence of carbon on the titania support. Indeed carbon-containing species have been observed to aid the reduction of titania (*12–14*). Furthermore, the chemical shift of TiC (+1.0 eV relative to Ti^0-$2p_{3/2}$) (*9, 15, 16*) precludes the unambiguous identification of this component in the complex spectra obtained after reduction at 973 K. However, close observation of the carbon signal during this reduction showed that the surface carbon signal remained unchanged in amount and type, suggesting that it does not participate in the reduction process. While the possible effects of carbon in the reduction of titania remain unclear at present, the observation that the Ti^{4+} in the iron-containing sample reduces at a significantly lower temperature (875 K) than in the TiO_2 film itself (with both samples containing the same amount of carbon) indicates that iron must play a role in this reduction process.

Spectral area analysis. A more quantitative discussion of the photoelectron spectral area changes is made possible by Fig. 6. In order to cancel effects due to small changes in the spectrometer detection electronics and sample positioning over several days of operation, the ratio of the Ti-$2p_{3/2}/2p_{1/2}$ spectral area to the Fe-$2p_{3/2}$ spectral area was computed. Since the $2p_{3/2}$ photoelectrons of iron and the $2p_{3/2}/2p_{1/2}$ photoelectrons of titanium have similar kinetic energies this procedure also canceled the effect caused by the uniform removal of a thin carbonaceous overlayer during low-temperature hydrogen treatment, as discussed earlier. After normalizing this ratio to unity for the initial iron overlayer (before treatment in hydrogen), the Ti/Fe area ratio is plotted versus hydrogen reduction

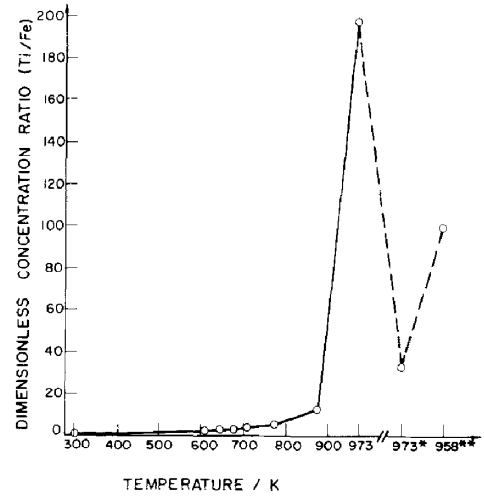

FIG. 6. Ti/Fe photoelectron spectral area ratio, normalized to unity for the initial iron overlayer (300 K), following reduction of 5-nm Fe/TiO_2 at the indicated temperatures. Broken portion of the Figure will be discussed in Part III. *, Oxidation; **, re-reduction at the indicated temperatures.

temperature in Fig. 6 for the 5-nm iron-on-titania sample. During nucleation of the iron overlayer into discrete iron particles, the Ti/Fe spectral area ratio increases smoothly to a value of approximately 4 (at 707 K). Further treatment at 773 K or higher temperatures leads to more dramatic increases in the Ti/Fe area ratio. Similar results were obtained for the 3.8-nm iron sample. Since this behavior cannot be attributed to sintering of the iron particles (as discussed in Part I), these spectral area ratio increases must be due to diffusion of iron into the support and/or reduction of Ti^{4+} to a lower valence state. The first effect causes a decrease in the Fe spectral area and a corresponding increase in the Ti spectral area (due to the loss of Fe from the surface), and the second effect causes a preferential increase in the Ti spectral area due to support reduction. Indeed, the large increase in the Ti/Fe area ratio after treatment at 973 K is due to approximately equal, but opposite, changes in the individual Fe and Ti spectral areas. That is, while the absolute Fe area decreases by a factor of 10, the Ti area increases by a factor of approximately 10 following treatment at this temperature. This interrelationship between the diffusion of iron into the support and the reduction of Ti^{4+} to lower valence states will be addressed in the next section, where the results of CEMS are presented.

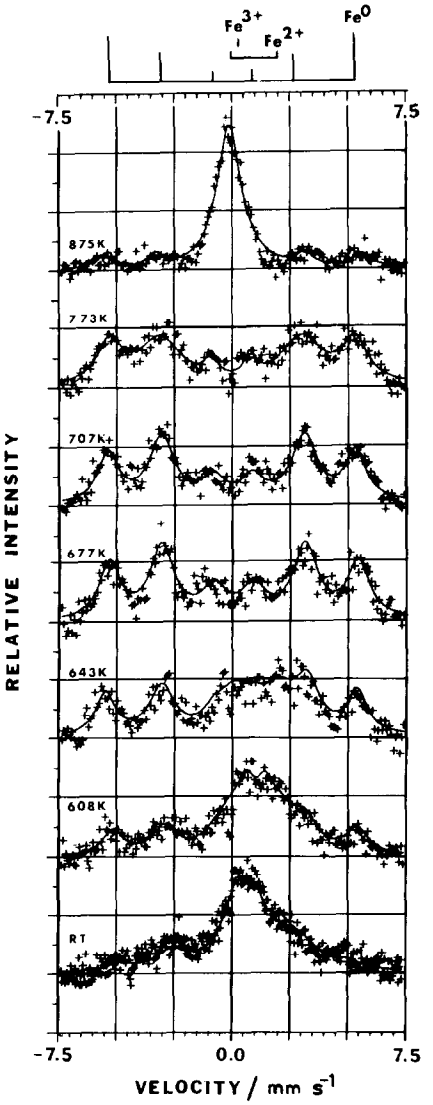

FIG. 7. Conversion electron Mössbauer spectra recorded from 5-nm Fe/TiO_2 specimen following reduction at the indicated temperatures. One vertical square is equivalent to 2% effect. (RT, initial iron overlayer)

CEMS Studies

Room-temperature conversion electron Mössbauer spectra for the 5-nm iron sample following the sequential reduction treatments of Table 1 of Part I are shown, along with their computer fits, in Fig. 7. A discussion of the spectra obtained from the 3.8-nm Fe/TiO_2 specimens (treated under similar conditions) is omitted as they were nearly identical to those of Fig. 7 except for subtle changes caused by a correspondingly smaller iron particle size. A weak spectral signal from stainless steel was observed in all spectra, corresponding to the Mössbauer spectrum of the vacuum chamber walls. This signal was constant during each series of experiments on a given sample, and it has been computer subtracted from the Mössbauer spectra of Fig. 7. The top of Fig. 7 also shows the expected peak positions of a magnetically split (sextuplet) metallic iron spectrum, a quadrupole doublet indicative of high-spin Fe^{2+}, and a spectral singlet for high-spin Fe^{3+}. The choice of a

quadrupole doublet for high-spin Fe^{2+} and a singlet for high-spin Fe^{3+} is based on the fact that the latter has a half-filled (symmetric) *d*-shell while the former does not. The possible contributions to the electric field gradient from, for example, surface or interface effects have not been considered in these qualitative peak positions at the top of the Figure.

Reduction at temperatures of 707 K *or lower.* A detailed analysis of the spectral changes accompanying reduction at temperatures below 677 K is complicated by the overlap between peaks due to Fe^{3+}, Fe^{2+}, and Fe^0 in the central region of the spectrum. The contributions from the Fe^0 peaks are easily resolved, since the positions and intensities of the outermost peaks of the sextuplet (that do not overlap with the peaks of Fe^{2+} and Fe^{3+}) can be used to calculate the positions and intensities of the innermost peaks of the sextuplet (that do overlap with the peaks of Fe^{2+} and Fe^{3+}). The spectral changes in the Fe^{2+} and Fe^{3+} components are more difficult to analyze. For Fe^{2+}, however, these changes can be fit to the model of Hobson (*17*). Accordingly, the Mössbauer spectrum of Fe^{2+} is composed of two quadrupole split doublets: one with a small splitting due to "coordinatively unsaturated" Fe^{2+} and another with a larger quadrupole splitting due to "highly coordinated" Fe^{2+}. For simplicity, the spectrum of Fe^{3+} is fit by a singlet. With these assumptions for Fe^{2+} and Fe^{3+} spectral components, the reduction process can be followed through computer analyses of the spectra. In short, it is found that the relative spectral areas (proportional to the relative amounts) of Fe^{3+}:Fe^{2+}:Fe^0 are 13:55:32% before hydrogen treatment, 0:59:41% after reduction at 608 K, 0:43:57% after treatment at 643 K, and 0:0:100% following reduction at 677 K. Accordingly, the Fe^{3+} is rapidly reduced to Fe^{2+} and Fe^0, followed by the slower reduction of Fe^{2+} to metallic iron. As suggested by XPS, the more difficult reduction of Fe^{2+} to metallic iron can be at least partially attributed to an interaction between Fe^{2+} and titania.

Finally, reference to Fig. 7 shows that further hydrogen treatment at 707 K does not lead to any spectral changes. Indeed, the spectral parameters of the sextuplet after treatment at either 677 or 707 (i.e., zero isomer shift and a magnetic hyperfine field of 330 kOe) are indicative of bulk metallic iron.

Reduction at 773 K. Hydrogen treatment at 773 K produces a significant broadening of the spectral peaks. Specifically, computer fitting this Mössbauer spectrum shows a 50% increase in the linewidths but no change in the isomer shift or magnetic hyperfine field, compared to the bulk metallic iron spectrum observed after treatment at 677 or 707 K. The results of transmission electron microscopy, presented in Part I of this series, showed that the iron particles spread over or wet the titania surface upon hydrogen treatment at 773 K. The increase in Mössbauer spectral linewidth following this same treatment is, in fact, consistent with this wetting phenomenon. For example, the occurrence of broad spectral lines in the magnetically split (i.e., six-peak) Mössbauer spectra of thin iron films (ca. 1 nm thick) has been reported in the literature, as recently reviewed by Mørup *et al.* (*18*). Applying these observations to the Fe/TiO_2 system, it can be said that the increased Mössbauer spectral linewidths upon treatment at 773 K are consistent with a transformation of three-dimensional iron crystallites into a "thin-crystal" morphology, caused when the particles spread over or wet the titania surface. Equally important, however, is the conclusion that the chemical state of iron does not change during this wetting process, since the isomer shift and magnetic hyperfine splitting of the iron sextuplet are the same as that of bulk metallic iron.

Reduction at temperatures of 875 K *or higher.* When the 5-nm iron sample is treated in hydrogen at 875 K, Fig. 7 shows that a dramatic change in the state of iron

takes place. Only traces of the metallic iron sextuplet remain (22% of spectral area) while the major new absorption appears at a position of approximately −0.14 mm/s. This peak position indicates that the iron in this new phase is present in the zero-valent state (as opposed to Fe^{2+} or Fe^{3+}). In addition, this iron must be strongly interacting with the support, as evidenced by the absence of room-temperature, magnetic hyperfine splitting and the negative displacement of the isomer shift from zero velocity. For example, while normal metallic iron (bcc α-Fe) shows a six-peak Mössbauer spectrum centered at zero velocity, phases such as FeTi or γ-Fe (fcc metallic iron) give single-peak Mössbauer spectra at approximately −0.15 mm/s. It is important to note that the formation of FeTi hydrides ($FeTiH_x$, $0 < x \leq 2$) can be discounted (*19*) as they would give rise to peaks in the Mössbauer spectrum at significantly higher velocities (e.g., peak at +0.12 mm/s for FeTiH and at +0.33 mm/s for $FeTiH_2$). Indeed, while Fe_2Ti does not hydride (*20*), the formation of FeTi hydrides is not expected at the temperatures and pressures employed in this study (*20*).

Another effect of the hydrogen treatment at 875 K is to decrease the total Mössbauer spectral area by approximately 30%. Since the recoil-free fraction of iron in FeTi or γ-Fe is expected to be comparable to that of bulk iron at room temperature (*21, 22*), it is suggested that this reduction in spectral area is caused by an attenuation of the conversion and Auger electrons which make up the Mössbauer spectrum. This attenuation results from the presence of iron atoms at depths below the surface on the order of the mean free paths of the detected electrons (*23–25*). Since it was shown in Part I that sintering of iron crystallites does not take place during hydrogen treatment at 875 K, the decrease in Mössbauer spectral area would be caused by the diffusion of iron into the support. This is in agreement with the results of XPS, which showed a decrease in the amount of iron present at the titania surface. Furthermore, TEM analyses indicated a decrease in the amount of iron present in discrete iron particles after hydrogen treatment at 875 K, and this suggests that the iron particles become dispersed into the support as opposed to being encapsulated by the support.

The previously discussed results of XPS indicated the presence of reduced titanium species on this iron-containing sample after reduction at 875 K. In fact, the reduction of the support and the diffusion of iron into the support may well be interrelated. On one hand, iron facilitates the reduction of Ti^{4+} to lower valence states, with the resulting formation of dispersed and strongly interacting iron. On the other hand, the removal of oxygen from the support during reduction of Ti^{4+} allows the iron to diffuse into the support.

Other Studies

Following the above CEMS studies, Auger electron spectroscopy was performed in the same chamber. These results indicated that carbon was the only detectable impurity, and its surface concentration was essentially the same as that found during XPS measurements. This validates the comparison of results from CEMS with results from XPS and TEM (the latter two techniques using samples treated in the same reaction chamber). In addition, the apparent agreement between the results of TEM and CEMS or XPS tends to discount the possible reducing effects of the metallic titanium backings present beneath both the CEMS and XPS specimens. More direct evidence that this metallic titanium backing does not alter the conclusions of the present study is obtained by noting the behavior of iron on commercial TiO_2 powders (*26, 27*). In particular, transmission Mössbauer spectroscopy has been used to study the interaction of iron with titania powders (50 m^2/g, Degussa) after hydrogen treatment at ca. 920 K. Of importance was the observation, for a 0.1 wt% Fe/TiO_2 sample, of a Mössbauer

spectral singlet at room temperature with parameters identical to those seen during the CEMS studies of Fig. 7.

Following high-temperature hydrogen treatment, Mössbauer spectra from the 0.1% Fe/TiO_2 powder were also collected at low temperatures (10 and 77 K) (*27*). A significant broadening of the apparent spectral singlet was observed, indicative of magnetic ordering at these temperatures. While it is not possible to unambiguously determine the nature of the iron-containing phase formed upon high-temperature hydrogen treatment, several qualitative statements can be made based on information in the literature: (i) stoichiometric, crystalline FeTi does not show the low-temperature magnetic ordering observed for these Fe/TiO_2 powders (*28*), (ii) iron clusters in various Fe_xTi ($1 \lesssim x \lesssim 2$) phases show low-temperature magnetic ordering (*28–32*), and (iii) γ-Fe also exhibits magnetic ordering consistent with that observed for these Fe/TiO_2 powders (*33*). This suggests that while hydrogen treatment at high temperature causes the iron to become dispersed into the support, some chemical bonding between iron atoms is retained, perhaps in the form of γ-Fe or Fe-containing clusters of Fe_xTi.

SUMMARY/CONCLUSIONS

The results of XPS and CEMS studies are summarized in Table 1. These investigations have verified and extended the conclusion from Part I of this series that the reduction of Fe/TiO_2 can be divided into three distinct temperature regimes. After reduction at temperatures less than or equal to 707 K, XPS and CEMS show that essentially all of the iron is in the metallic state, and its properties are those of bulk metallic iron. Hydrogen treatment at 773 K produces a broadening of the Mössbauer spectrum, consistent with the spreading of iron crystallites over the titania support. Finally, reduction at temperatures above ca. 875 K leads to decreases in the XPS and CEMS spectral iron areas. In addition, CEMS shows the formation of a new metallic species that does not show magnetic hyperfine splitting at room temperature; and, XPS shows that part of the Ti^{4+} is reduced to lower valence states. These observations suggest that upon high-temperature hydrogen treatment, the titania support undergoes reduction and iron diffuses into the support as a dispersed and strongly interacting species (e.g., γ-Fe or Fe_xTi, $1 \lesssim x \lesssim 2$). A detailed discussion of

TABLE 1

XPS and CEMS Reduction Summary (~5.0 nm Fe)

Reduction temperature (K)	Observed XPS trends	Observed CEMS trends	Reduction regimes
Initial iron overlayer	Fe^{3+}/Ti^{4+}	55% Fe^{2+}, 32% Fe^0, 13% Fe^{3+}	
608	Fe^0 and Fe^{2+}/Ti^{4+}	59% Fe^{2+}, 41% Fe^0	Low-temperature reduction, nucleation, and growth
643	Fe^0/Ti^{4+}	57% Fe^0, 43% Fe^{2+}	
677 707	Fe^0/Ti^{4+}	100% Fe^0	
773	Fe^0/Ti^{4+}	Fe^0, broadened spectrum	Spreading of iron over support
875	Decrease in Fe spectral area, increase in Ti spectral area, reduction of Ti^{4+}	Spectral singlet (e.g., γ-Fe, Fe_xTi); ~32% decrease in spectral area	Diffusion of iron into support
973			

TEM, XPS, and CEMS reduction studies is withheld until Part III of this series so that it may be combined with the behavior of Fe/TiO_2 during oxidation treatments.

ACKNOWLEDGMENTS

See the acknowledgments of Part III.

REFERENCES

1. Baker, R. T. K., Prestridge, E. B., and Garten, R. L., *J. Catal.* **56**, 390 (1979).
2. Baker, R. T. K., Prestridge, E. B., and Garten, R. L., *J. Catal.* **59**, 293 (1979).
3. Tatarchuk, B. J., and Dumesic, J. A., *J. Catal.* **70**, 308 (1981).
4. Greenwood, N. N., and Gibb, T. C., "Mössbauer Spectroscopy." Chapman & Hall, London, 1971.
5. Sørensen, K., *in* "LTE. II. Internal Report No. 1, 1972." Laboratory of Applied Physics II, Technical University of Denmark, Lyngby.
6. Topsøe, H., Dumesic, J. A., and Mørup, S., *Appl. Mössbauer Spectrosc.* **2**, 55 (1980).
7. Franzen, H. F., Umana, M. X., McCreary, J. R., and Thorn, R. J., *J. Solid State Chem.* **18**, 363 (1976).
8. Ramqvist, L., Hamrin, K., Johansson, G., Fahlman, A., and Nordling, C., *J. Phys. Chem. Solids* **30**, 1835 (1969).
9. Wagner, C. D., Riggs, W. M., Davis, L. E., and Moulder, J. F., *in* "Handbook of X-ray Photoelectron Spectroscopy" (G. E. Muilenberg, Ed.). Perkin–Elmer Corporation, 1979.
10. Armstrong, N. R., and Quinn, R. K., *Surface Sci.* **67**, 451 (1977).
11. Sayers, C. N., and Armstrong, N. R., *Surface Sci.* **77**, 301 (1978).
12. Iyengar, R. D., and Codell, M., *Advan. Colloid Interface Sci.* **3**, 365 (1972).
13. Gebhardt, J., and Herrington, K., *J. Phys. Chem.* **62**, 120 (1958).
14. Iyengar, R. D., and Kellerman, R., *Z. Phys. Chem. (Frankfurt am Main)* **64**, 345 (1969).
15. Ihara, H., Kumashiro, Y., Itoh, A., and Maeda, K., *Japan. J. Appl. Phys.* **12**, 1462 (1973).
16. Johansson, L. I., Hagström, A. L., Jacobson, B. E., and Hagström, S. B. M., *J. Electron Spectroscopy Relat. Phenom.* **10**, 259 (1977).
17. Hobson, M. C., *Progr. Surf. Membr. Sci.* **5**, 1 (1972).
18. Mørup, S., Dumesic, J. A., and Topsøe, H., *Appl. Mössbauer Spectrosc.* **2**, 1 (1980).
19. Swartzendruber, L. J., and Bennett, L. H., *Bull. Amer. Phys. Soc.* **21**, 272 (1976).
20. Sandrock, G. D., Reilly, J. J., and Johnson, J. R., "Applications of Phase Diagrams in Metallurgy and Ceramics." NBS Special Publication SP-496, 1977.
21. Steyert, W. A., and Taylor, R. D., *Phys. Rev. A* **134**, 716 (1964).
22. Stupel, M. M., Ron, M., and Weiss, B. Z., *J. Appl. Phys.* **47**, 6 (1976).
23. Tatarchuk, B. J., and Dumesic, J. A., to be published.
24. Krakowski, R. A., and Miller, R. B., *Nucl. Instrum. Methods* **100**, 93 (1972).
25. Huffman, G. P., *Nucl. Instrum. Methods* **137**, 267 (1976).
26. Garten, R. L., private communication.
27. Tatarchuk, B. J., and Dumesic, J. A., to be published.
28. Wertheim, G. K., and Wernick, J. H., *Acta Met.* **15**, 297 (1967).
29. Narayanasamy, A., Ericsson, T., Nagarajan, T., and Muthukumarasamy, P., *Phys. Status Solidi A* **42**, K65 (1977).
30. Brückner, W., Kleinstück, K., and Schulze, G. E. R., *Phys. Status Solidi A* **1**, K1 (1970).
31. Wertheim, G. K., Wernick, J. H., and Sherwood, R. C., *J. Appl. Phys.* **41**, 1325 (1970).
32. Wertheim, G. K., Buchanan, D. N. E., and Wernick, J. H., *Solid State Commun.* **8**, 2173 (1970).
33. Gonser, U., Meechan, C. J., Muir, A. H., and Wiedersick, H., *J. Appl. Phys.* **34**, 2373 (1963).